LCL-filter Design for Robust Active Damping in Grid Connected Converters

Rafael Peña-Alzola, Marco Liserre, *Fellow, IEEE,* Frede Blaabjerg, *Fellow, IEEE,* Martin Ordonez, *Member, IEEE,* and Yongheng Yang, *Student Member, IEEE*

***Abstract*—Grid connected converters employ *LCL*-filters, instead of simple inductors, because they allow lower inductances while reducing cost and size. Active damping, without dissipative elements, is preferred to passive damping for solving the associated stability problems. However, large variations in the grid inductance may compromise system stability, and this problem is more severe for parallel converters. This situation, typical of rural areas with solar and wind resources, calls for robust *LCL*-filter design. This paper proposes a design procedure with remarkable results under severe grid inductance variation. The procedure considers active damping using lead-lag network and capacitor current feedback. Passive damping is also discussed. The design flow, with little iteration and no complex algorithms, selects the proper ratios between the switching and resonance frequency, the grid and converter inductance, and the filter capacitance and total inductance. An estimation for the grid current THD is also proposed. Simulation and experiments validate the proposals.**

***Index Terms*—grid connected converter, *LCL*-filter, stability, robust design, active damping, weak grid.**

I. Introduction

GRID connected converters supply sinusoidal currents and employ either a simple inductor or an *LCL*-filter to limit the current ripple [1]. Using an *LCL*-filter results in lower inductance values and so allows a more compact design and lower losses. Because of these advantages, this solution is now used widely in distributed generation (solar and wind) [2], [3] and power active filters [4]. However, the current control in closed loop may be unstable because of the *LCL*-filter resonance [5]. Passive damping solves this issue by using simple resistors at the expense of additional losses [6], [7]. Active damping modifies the control algorithm without using dissipative elements [8].

References [9], [10] established the basic guidelines for the selection of the *LCL*-filter parameters using an iterative process. The converter-side inductor is sized based on the current ripple at the switching frequency. The capacitor rating is limited by the fundamental reactive power. The grid side converter is selected to further reduce the current ripple. In [11], the wye and delta connections are also considered. The analytical solution of the converter harmonics is used in [12], and the minimum energy stored in *LCL*-filter is selected as optimization criterion. In [13], [14] two parallel capacitors, one of them with a series resistor for passive damping, are considered. Reference [13] makes use of simple approximations to obtain the *LCL*-filter parameters that comply with the grid requirements and while causing the most minimal losses. In [14], after modeling all the losses with high accuracy, a search algorithm enables the calculation of the optimal *LCL*-filter values that result in the lowest volume and losses. In [15], the integration of both inductors in one single core is proposed. Reference [16] uses a graphic approach for an *LCL*-filter that is intended to work in a shunt active power filter.

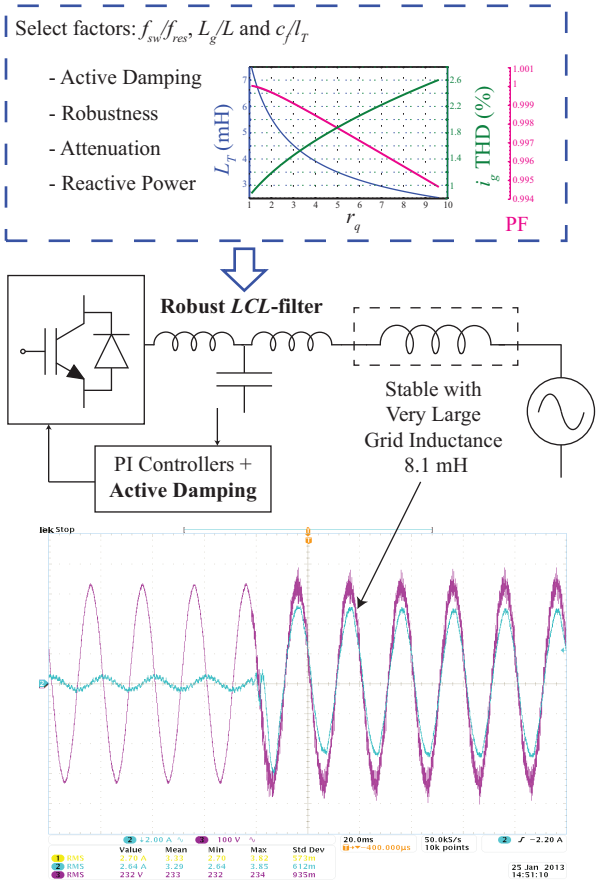

Fig. 1. Conceptual procedure and results of the proposed *LCL*-filter design method.

R. Peña-Alzola and M. Ordonez are with the department of Electrical and Computer Engineering, The University of British Columbia. 2332 Main Mall, Vancouver V6T 1Z4, BC Canada. E-mail: rafaelpa@ece.ubc.ca, mordonez@ieee.org

M. Liserre is with the Institute for Power Electronics Electronics and Electrical Drives, Christian-Albrechts-University of Kiel, 24143 Kiel, Germany. E-mail: ml@tf.uni-kiel.de

F. Blaabjerg and Y. Yang are with Department of Energy Technology, Aalborg University. Pontoppidanstrde 101, 9220 Aalborg, Denmark. E-mail: {fbl, yoy}@et.aau.dk

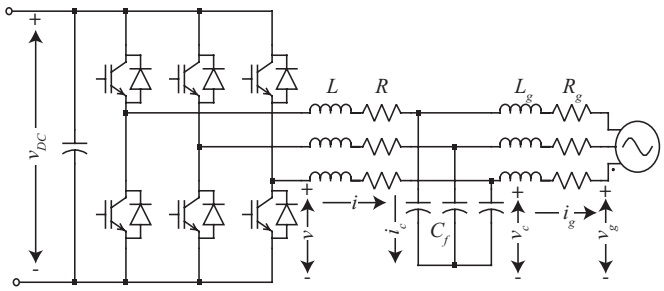

Fig. 2. *LCL*-filter based three phase inverter.

A vast amount of literature on the active damping of *LCL*-filters is available [3], [4], [6], [17]–[32]. Earlier methods use a feedback loop additional to the usual PI current control [23]. The feedback magnitude was the grid current derivative [24], the capacitor current [23], [33] or the capacitor current filtered by lead-lag network [6], [19], [22]. The use of a notch filter at the output of the voltage reference to the PWM modulator was proposed in [20], [21], [34]. In [34] a self-commissioning procedure for tuning the notch filter to the measured resonance frequency is proposed. The virtual resistor method [31] emulates the behavior of a resistor without adding it physically. Recent methods propose state feedback with linear [27], [28], non-linear [29] and adaptive control [30].

The variations in the resonance frequency, caused by weak grids with large inductance variations, may compromise system stability [25]. Remote rural areas, typical locations of renewable resources, are characterized by low power transformers and long distribution wires that result in weak grids with high impedance. Moreover, this situation is aggravated by the increasing connection of grid converters [35], [36] in parallel, which has raised new stability problems because of the newly arising resonances. Ref. [37] shows that, when converters with very similar characteristics are connected in parallel, the equivalent grid inductance is multiplied by the number of converters. Therefore, in view of wind parks and solar farms located in remote rural areas, with weak grids and numerous converters in parallel, this paper proposes an *LCL*-filter design procedure that aims to achieve robustness in the face of large inductance variations.

This paper proposes a simple design procedure that enables *LCL*-filters to obtain enhanced stability and robust results based on selecting the ratios between the switching and resonance frequency, the grid and converter inductance, and the filter capacitance and total inductance. The main novelty is the integration of the damping procedure with the *LCL*-filter design to achieve maximum robustness in the face of grid inductance variations. This robustness is due to the importance of the ratio between the switching and resonance frequency for the damping procedures. The proposed robust *LCL*-filter design is applicable to active damping using lead-lag network and capacitor current feedback. Passive damping, achieved by inserting resistors in series with the capacitors of the *LCL*-filter, is also explained. The derivation of the ratio between the switching and resonance frequency for the capacitor current

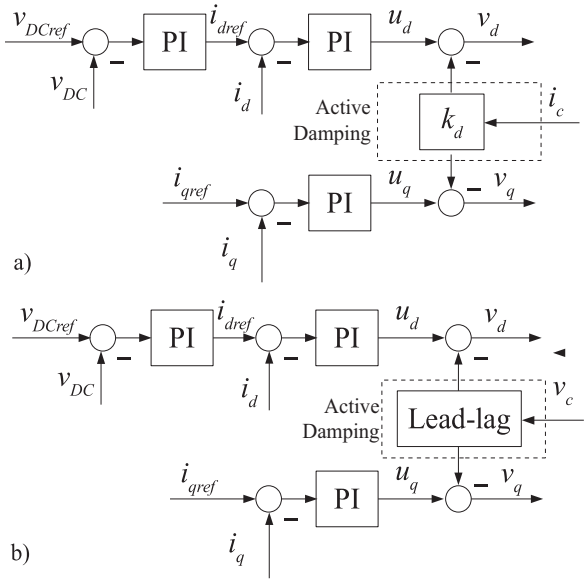

Fig. 3. Cascade control of the grid converter with active damping: a) capacitor current feedback and b) lead-lag network.

feedback is shown. The effects of the ratio between the grid and converter inductance on the harmonic attenuation and on the robustness of the *LCL*-filter is explained. In addition, an estimation for the grid current THD is proposed. All the equations derived are simple and accurate, and provide the insight needed to make the necessary trade-off in designing the *LCL*-filter. This enables the calculation of all the parameters in a simple design flow with little iteration and without complex algorithms. Analysis in the z-plane is used to assess the stability and robustness against the parameter variation. Fig. 1 shows the main achievement of the proposed procedure:

- The parameters of the robust *LCL*-filter are obtained by simply selecting the proper ratios by considering the active damping method, the attenuation, the robustness, and the reactive power consumption.
- The *LCL*-filter converter is stable even in the presence of a very large grid inductance.

The paper is organized as follows: Section II succinctly reviews the control for grid connected converter based on the *LCL*-filter. Section III explains considerations for the *LCL*-filter design. Section IV. provides a step-by-step procedure for implementing the *LCL*-filter, along with examples. Simulations are shown in Section V and experiments in Section VI. Finally, conclusions are presented in Section VII.

II. Control of Grid Connected Converters: Background Review

Fig. 2 shows an *LCL*-filter based three-phase inverter. For the power range of kW-MW, the current sensors are usually integrated into the converter for protection [10]. The value of grid inductance L_g includes the inductance of the grid side inductor and the leakage inductance of the isolation transformer, both assumed to be known, and the line inductance, assuming to be unknown.

In this paper, the converter side current is the one sensed for control. Fig. 3 shows the cascade control used for grid connected converters. In the low frequency region, the *LCL*-filter behaves approximately as an equivalent *L*-filter, as a result of the neglect of the capacitor branch [19]. Therefore, the usual formulas for tuning the controllers when using an *L*-filter can also be employed when using an *LCL*-filter. The synchronization with the grid voltage is obtained by means of a PLL [38]. The *LCL*-filter based converter uses the same PI-controllers, tuned following the same procedures, as does the *L*-filter based counterpart. The current control in the *dq*-frame uses simple PI controllers tuned according to the technical optimum criterion [22], with the following proportional gain and integration time:

$$K_p = \frac{L_T f_{sw}}{3} \tag{1}$$

$$T_i = \frac{L_T}{R_T} \tag{2}$$

with $L_T = L + L_g$ the sum of the converter and grid inductor inductances (L and L_g respectively), $R_T = R + R_g$ the sum of the converter and grid resistances (R and R_g respectively) and f_{sw} the switching frequency. The bandwidth achieved is $f_{bw} \approx f_{sw}/20$. As (2) is usually large, the integration time can be reduced for better disturbance rejection, provided the overshoot is still acceptable [39]. The *d*-current performs the DC voltage regulation, whereas the *q*-current controls the reactive power, usually to achieve unity power factor. The grid voltage feed-forward and *dq*-current uncoupling terms are omitted in Fig. 3 for clarity.

III. Considerations for the *LCL*-filter Design

A. Ratio between the switching and resonance frequency

The active damping methods considered for the *LCL*-filter design are the capacitor current feedback, Fig. 3a, and the lead-lag network, Fig. 3b. When using these active damping methods, the ratio $r_f = f_{sw}/f_{res}$ between the switching frequency and the resonance frequency, f_{res} has crucial importance.

In general, f_{res} should be halfway between f_{bw} and f_{sw}. In this way, the resonance does not interfere with the current control loop, while the *LCL*-filter provides proper harmonic reduction [9]. Therefore, by taking the geometric mean between f_{bw} and f_{sw} for f_{res}, the appropriate ratio should be around $r_f \approx 4.5$.

For grid current control with $r_f < 6$ [26], no active damping method is necessary to achieve stability. For the lead-lag network, it was shown in [19] that the required ratio should be $r_f \approx 3.2$–3.4.

For capacitor current feedback, it will be shown in the following subsection that the required ratio should be $r_f \approx 3$.

The resonance frequency is equal to:

$$f_{res} = \frac{f_{sw}}{r_f} = \frac{1}{2\pi}\sqrt{\frac{1}{C_f}\left(\frac{1}{L} + \frac{1}{L_g}\right)} \tag{3}$$

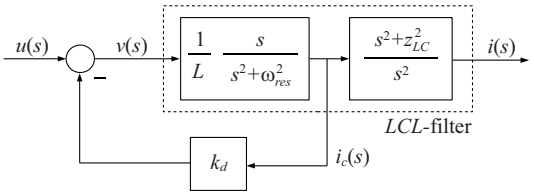

Fig. 4. *LCL*-filter with capacitor current feedback for active damping.

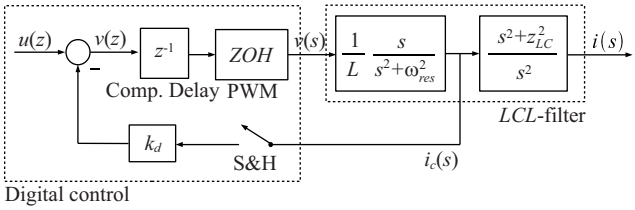

Fig. 5. Digital implementation of the capacitor current feedback.

where C_f is the filter capacitance. Thus, from (3) for a constant f_{sw}, larger r_f requires larger passive elements.

For the capacitor current feedback, see Fig. 4, the transfer function relating the converter current i and the converter voltage reference u is:

$$G_{ad}(s) = \frac{i(s)}{u(s)} = \frac{1}{Ls}\frac{s^2 + z_{LC}^2}{s^2 + 2\underbrace{\left[\frac{k_d}{2L\omega_{res}}\right]}_{active\ damping}\omega_{res}s + \omega_{res}^2} \tag{4}$$

where $z_{LC}^2 = [L_g C_f]^{-1}$ and $\omega_{res}^2 = (2\pi f_{res})^2 = (1 + L_g/L)z_{LC}^2$. It can be seen that the damping in (4) is varied by varying the feedback gain k_d. This is analogous to what happens with passive damping when varying the value R_d of the damping resistor in series with the *LCL*-filter capacitor. The transfer function relating the converter current i and voltage v for passive damping is:

$$G_{pd}(s) = \frac{i(s)}{v(s)} = \frac{1}{Ls}\frac{s^2 + 2\zeta' z_{LC}s + z_{LC}^2}{s^2 + 2\underbrace{\frac{C_f\omega_{res}}{2}R_d}_{passive\ damping}\omega_{res}s + \omega_{res}^2} \tag{5}$$

and the damping in (5) can be varied with R_d. Unlike (4), (5) has zeros with damping $\zeta' = R_d(C_f z_{LC})/2$. By considering the minimum damping resistor for stability established in [40], and after introducing the ratios r_l and r_f, the minimum damping for stable closed-loop poles is:

$$\zeta'_{min} = \frac{1}{12\pi} r_f \frac{r_l}{\sqrt{1 + r_l}} \tag{6}$$

with $r_l = L_g/L$. For the usual values of r_f and r_l and considering that R_d is limited by the damping losses, the zeros in (5) are slightly damped ($\zeta' << 1$). Therefore, (4) and (5) will behave similarly.

The Padé approximant $p_{N,M}(x)$ of a function $f(x)$ is a quotient of two polynomials, with degrees N and M, having

the same Taylor series expansion up to degree $M+N$ [41]. The Padé approximant is simple to calculate and allows to use the tuning formulas for PI controllers (1)-(2). When considering the capacitor current feedback, the Padé approximant $p_{0,1}(x)$ (same order as an *L*-filter) of (4) (including the inductor resistances) can be used as an equivalent model for the low frequency region $\omega << \omega_{res}$:

$$G_{adlf}(s) = \frac{i(s)}{u(s)} = \frac{1}{(L + L_g - R_g^2 C_f + k_d C_f R_g)s + (R + R_g)} \tag{7}$$

This is almost the same as neglecting the capacitor branch in the *LCL*-filter, since the additional terms are very small.

The digital implementation of the capacitor current feedback incorporates lag phase shifts due to the computational and PWM delays, see Fig. 5. It is considered that all the calculations (PI controllers and active damping procedure) take one PWM cycle (the sampling and the PWM are synchronous). This is usually the case with DSP and rapid prototyping tools such as dSpace that are used to produce experimental results [8]. In the *s*-domain, the transfer function modeling the effects of the computational delay and the PWM is [42]:

$$G_d(s) = e^{-T_s s}\frac{1 - e^{-T_s s}}{T_s s} \tag{8}$$

with $T_s = 1/f_{sw}$, the sampling period coincident with the switching period. The first product of (8), a pure delay, models the computational delay. The second product of (8) models a ZOH equivalent to the PWM for control modeling purposes [21]. The effect of the computational delay and PWM at the resonance frequency can be studied by substituting $s = j\omega_{res}$ in (8):

$$G_d(j\omega_{res}) = e^{-T_s j\omega_{res}}\frac{1 - e^{-T_s j\omega_{res}}}{jT_s\omega_{res}} \tag{9}$$

which can be factorized as [42]:

$$G_d(j\omega_{res}) = \operatorname{sinc}\left(\frac{T_s}{2}\omega_{res}\right)e^{-\frac{3T_s}{2}j\omega_{res}} \tag{10}$$

According to (10), the effects of the PWM and computations at the resonance frequency are a gain, first factor, and a pure delay, second factor. By selecting $\omega_{res} = 2\pi/3T_s$, (10) the pure delay produced by the PWM and computations is null and the gain results in:

$$G_d(j\omega_{res}) = -3\frac{\sqrt{3}}{2\pi} \tag{11}$$

Hence, the digital implementation delays at the resonance frequency, where damping is necessary, can be compensated for by simply inverting (11). Selecting $\omega_{res} = 2\pi/3T_s$, (10) corresponds to the ratio between the resonance and the sampling frequency $r_f = f_{sw}/f_{res} = 3$. For the general case, by separating the real and imaginary components of (10):

$$k_d G_d(j\omega_{res}) = k_d \operatorname{sinc}\left(\frac{T_s}{2}\omega_{res}\right)\left[\cos\left(-\frac{3T_s}{2}\omega_{res}\right) + j\sin\left(-\frac{3T_s}{2}\omega_{res}\right)\right] \tag{12}$$

with k_d the feedback gain of the capacitor current. The only feedback component of (12) that produces active damping is the real part in phase with the capacitor current at the resonance frequency. Therefore, the condition to obtain active damping is:

$$k_d \Re\left\{G_d(j\omega_{res})\right\} = k_d \operatorname{sinc}(\pi/r_f)\cos(3\pi/r_f) > 0 \tag{13}$$

In order to make (13) positive, up to the maximum ratio $r_f = 6$, the gain k_d should be negative. For higher r_f, the gain k_d must be positive to fulfill (13) and the computation and PWM delays can be considered negligible. The minimum ratio should be $r_f = 2$, as the sampling frequency should be higher than the resonance frequency so that the resonance is visible to the digital control. This finding is consistent with [18], where the same ratios r_f and signs for k_d are obtained by applying the Jury's criterion to the digital implementation of the capacitor current feedback. By setting the derivative of (13) with respect to r_f equal to zero, the optimal value for $r_f \approx 3.12$ is obtained, which results in maximum real part of (12) and so maximum damping at the damping frequency. This value is very close to the previously $r_f = 3$, which resulted in canceling the pure delay in (10).

B. Ratio Between the Grid and Converter Inductance

The ratio r_l refers to the quotient between the known part L_g (corresponding to the grid side inductor and the isolation transformer), and L (corresponding to the converter side inductor). The ratio between the grid and converter inductance values $r_l = L_g/L$ affects total attenuation of the *LCL*-filter. In addition, it will be shown that the ratio also affects the variation of the resonance frequency when the grid inductance varies.

In equation (3), by substituting f_{res} with f_{sw}/r_f, L with $L_T/(1 + r_l)$ and L_g with $L_T r_l/(1 + r_l)$ where $L_T = L_g + L$ the total inductance and $r_l = L_g/L$ the ratio between the grid and converter side inductance, the result is:

$$L_T C_f = \frac{1}{4\pi^2}\frac{r_f^2}{f_{sw}^2}\frac{(1 + r_l)^2}{r_l} \tag{14}$$

With constant f_{sw}, the value of the product $C_f L_T$ is minimum for $r_l = 1$, by setting the derivative of (14) with respect to r_l equal to zero. This means that the passive elements will have a minimal size when $r_l = 1$ ($L = L_g$) is selected. Therefore, whatever the selection of C_f, selecting $r_l = 1$ results in the minimum total inductance L_T. The minimum L_T implies that there will be a minimum voltage drop, and so a higher dynamic response. Conversely, whatever the selection of L_T, $r_l = 1$ also results in the minimal requirement for capacitor C_f, as was shown in [13], and therefore in minimal reactive power. In addition, equal inductors may

be economically advantageous. However, the attenuation of the *LCL*-filter at the switching frequency, by considering the transfer function relating the converter voltage v and the grid current i_g, is found to be:

$$\frac{i_g(f_{sw})}{v(f_{sw})} = 2\pi \frac{C_f f_{sw}}{r_f^2(r_f^2-1)} \frac{r_l}{(1+r_l)^2} \tag{15}$$

and the ratio $r_l = 1$ corresponds to the minimum attenuation. Nevertheless, variations of r_l between 0.5 and 2 results in variations in the attenuation (15) of just 12%.

The ratio r_l also influences the per unit variation of f_{res} related to the per unit variation of the *LCL*-filter inductance according to:

$$\frac{\frac{df_{res}}{f_{res}}}{\frac{dL_g}{L_g}} = -\frac{1}{2}\frac{1}{1+r_l} \tag{16a}$$

$$\frac{\frac{df_{res}}{f_{res}}}{\frac{dL}{L}} = -\frac{1}{2}\frac{r_l}{1+r_l} \tag{16b}$$

by deriving f_{res} in (3) with respect to L_g and L respectively. According to (16), increasing r_l results in increased robustness in the face of the grid inductance variations L_g. The detrimental effect for the robustness of the converter inductance is not problematic, as L is a known parameter and not likely to vary. However, the value of r_l should not be increased very much, in order to prevent the overall inductance L_T becoming excessively large in (14). The ratio r_l has no effect on the per unit variation of the *LCL*-filter variation:

$$\frac{\frac{df_{res}}{f_{res}}}{\frac{dC_f}{C_f}} = -\frac{1}{2} \tag{17}$$

by deriving f_{res} in (3) with respect to C_f. Thus, the robustness against the resonance frequency variation caused by the capacitor variations can only be increased by increasing the capacitance C_f.

C. Ratio between the LCL-filter inductance and capacitance

The last ratio to be selected is related to the reactive power produced by the *LCL*-filter capacitor. In order to achieve unity power factor at the point of common coupling (PCC), the converter needs to compensate for the reactive power produced by the filter capacitor. Assuming the rated grid current $I_g = I_n$ in phase with the rated voltage $V_g = V_n$ at the PCC, by doing phasor calculations the converter voltage and current are found to be $v = (1-c_f l)+j(l+l_g-c_f l l_g)$ and $i = (1-c_f l_g)+jc_f$ respectively, with lower letters indicating per unit values. The selected base values for the per unit system are $S_b = S_n$, with S_n the rated power, $V_b = V_n$ with V_n the rated ac voltage, and $f_b = f_n$ with f_n the grid fundamental frequency. The derived base values are $C_b = 1/(Z_b\omega_b)$ and $L_b = Z_b/\omega_b$ with $Z_b = V_b^2/S_b$ and $\omega_b = 2\pi f_b$. Hence, the active power injected by the converter is $p = 1$ pu and the reactive power is:

$$q = c_f(1+c_f l) - (1-c_f l_g)(l+l_g-c_f l l_g) \approx c_f - l_T \tag{18}$$

For other power factor values at the PCC, the following analysis is analogous. The last approximation in (18) assumes the rated current I_n circulating through both inductors L and L_g an the rated voltage V_n across the capacitor C_f.

The reactive power production implies an increase in the converter rating. In order not to over-rate the converter, c_f should be equal to l_T according to (18). Defining the ratio $r_q = c_f/l_T = Z_b^2 C_f/L_T$, this is the same as selecting $r_q = 1$. However, this may result in very low capacitance and excessively large inductance values. This implies bulky and expensive inductors and prevents the *LCL*-filter from providing any substantial advantage compared to the simple *L*-filter. In order to reduce the inductance values, $r_q = c_f/l_T$ should be increased but not so as to make the resulting capacitance too large. Hence, the reactive power q should be small, with a power factor PF at the converter terminals higher than 0.995. This corresponds to a reactive power $q = 0.1$ pu with a converter overrating of $s = \sqrt{1+q^2} = 1/\text{PF}$ pu, less that 1%. The reactive power q is related to r_q, by substituting r_q and (18) in the per unit version of (14), according to the following expression:

$$q = \frac{(r_q-1)}{\sqrt{r_q}} \frac{(1+r_l)}{\sqrt{r_l}} \frac{r_f f_n}{f_{sw}} \tag{19}$$

and the power factor PF at the converter output is:

$$\text{PF} = \frac{\text{real power}}{\text{apparent power}} = \frac{1}{\sqrt{1+q^2}} \approx 1 - \frac{q^2}{2} \tag{20}$$

The stored energy in the *LCL*-filter can be considered as a measure for the size and expense of the passive components. The total filter energy can be approximated by [12]:

$$W_t = \frac{3}{2}\left(L_T I_n^2 + C_F V_n^2\right) \tag{21}$$

The stored energy, in the per unit system, is:

$$w_t = \frac{3}{2}(l_T + c_f) \tag{22}$$

The total inductance per unit, by taking into account $r_q = c_f/l_T$ in (14), is:

$$l_T = r_f \frac{f_n}{f_{sw}} \frac{1+r_l}{\sqrt{r_l r_q}} \tag{23}$$

The stored energy in the per unit system, by substituting (23) and $r_q = c_f/l_T$ in (22), is:

$$w_t = \frac{3}{2} l_T (1+r_q) = \frac{3}{2} r_f \frac{f_n}{f_{sw}} \frac{1+r_l}{\sqrt{r_l}} \frac{1+r_q}{\sqrt{r_q}} \tag{24}$$

The ratio $r_l = 1$ corresponds to the minimum stored energy, by setting the derivative of (24) with respect to r_l equal to zero. This result was expected, as $r_l = 1$ resulted in minimum product $L_T C_f$ in (14). The ratio $r_q = 1$ corresponds to the minimum stored energy, once more, by setting the derivative with respect to r_f to zero. For values $r_q > 1$ the stored energy, in pu, increases slightly, and almost linearly.

D. Estimation for Total Harmonic Distortion of the Grid Current

This subsection proposes an estimation of the grid current THD (total harmonic distortion) in order to assess that attenuation of the *LCL*-filter. A study on how the different ratios affect the grid current THD is also shown. Finally, the proposed formulas allow the losses of the passive damping case to be studied.

Lower and higher bounds for rms value of the capacitor current, based on the negligible impedance path in the capacitor branch, were established in [40] as follows:

$$\tilde{i}_c^{low} = \frac{1}{2\sqrt{3}}\frac{1}{\sqrt{48}}\frac{v_{DC}}{f_{sw}L}\sqrt{\frac{3}{2}m^2 - \frac{3\sqrt{3}}{\pi} + \frac{9}{8}\left(\frac{3}{2} - \frac{9}{8}\frac{\sqrt{3}}{\pi}m^4\right)} \tag{25a}$$

$$\tilde{i}_c^{up} = \tilde{i}_c^{low}\left|\frac{s^2}{s^2+\omega_{res}^2}\right|_{s=j[(m_f-6)\omega_n]} \tag{25b}$$

with m the modulation index, $\omega_n = 2\pi f_n$, $m_f = f_{sw}/f_n$ the frequency modulation ratio and v_{DC} the dc link voltage. By assuming negligible current harmonic for order $m_f - 6$, an upper bound for the rms value of the grid current can be obtained by considering the transfer function relating i_g and i_c in the *LCL*-filter:

$$\tilde{i}_g^{up} = \tilde{i}_c^{up}\left|\frac{i_g(s)}{i_c(s)}\right|_{s=j[(m_f-6)\omega_n]} = \tilde{i}_c^{up}\frac{z_{LC}^2}{\left[(m_f-6)\omega_n\right]^2} \tag{26}$$

The previous equations assume ideal conditions, with no harmonic content in the grid voltage, ideal power switches and passive elements and constant dc link voltage, which enables the attainment of a simple approximation. Hence, even though it is an upper bound estimation, the result of (26) is optimistic, and in order to account the previous factors, additional margin should be considered. Dividing (26) by the rated current I_n (rms values of the fundamental current harmonic) results in an approximate THD of the grid current. Aggregating all the factors in (26) results in:

$$\tilde{i}_g^{up} = \frac{1}{24}\frac{v_{DC}}{f_{sw}LL_gC_f}\frac{1}{(m_f-6)^2\omega_n^2 - \omega_{res}^2}f(m) \tag{27}$$

where $f(m)$ refers to the terms under the square root in (25). By substituting (14) in (27) and incorporating the factors r_f, r_l and r_q the upper bound of the grid current is found to be as follows:

$$\tilde{i}_g^{up} = \frac{\pi v_{DC}}{12Z_b}\frac{\sqrt{r_q}}{r_f^3}\frac{\sqrt{r_l}}{(1+r_l)}\frac{1}{\left[(1-6/m_f)^2 - 1/r_f^2\right]}f(m) \tag{28}$$

Eq. (28) summarizes the effects of all the defined coefficients in the grid current THD. Increasing r_f reduces the grid current THD substantially, as the switching frequency is further in the 60 dB/decade region. Increasing r_q, to decrease L_T by increasing C_f, slightly decreases the *LCL*-filter effectiveness. Therefore, in selecting r_q, the reactive power must not overrate the converter, see (19)-(20), and the requirements for the grid current THD must be fulfilled, see (28). Finally, variations in r_l are also lenient for the grid current THD as explained previously.

Previous derivations assume an overall *LCL*-filter behavior as described in (4) and (5). The rationale for the lead-lag network method uses (4); details can be found in [19]. The procedure basically consists of the feedback of the approximate derivative of the capacitor voltage. This is the same as feeding back the component of capacitor current at the resonance frequency, where damping is needed. Hence, the lead-lag network method will result in a less robust response to resonance frequency variations when compared to the capacitor current feedback method. In addition, the transfer function is considerably modified, with a behavior that departs from (4) and, in the case of the lead-lag network, the previous formulas are less accurate.

For passive damping, the minimum damping resistor for stability, $R_d = f_{sw}L_g^2/3(L+L_g)$ [40], and the approximation (25b) enables the study of the effects of the different parameters in the damping losses $P_d = R_d\tilde{i}_c^2$:

$$P_d \approx \frac{\pi v_{DC}^2}{864Z_b}\frac{\sqrt{r_q}}{r_f}\frac{\sqrt{r_l}r_l^2}{(1+r_l)}\frac{(1-6/m_f)^4 f^2(m)}{(1-1/r_f^2-12/m_f+36/m_f^2)^2} \tag{29}$$

Eq. (29) is again obtained by incorporating the factors r_f, r_l and r_q to (25b). Therefore, elevated r_f should be considered for passive damping in order to reduce the losses with moderate r_l.

IV. Step-by-step Design Procedure for the *LCL*-filter

A. Design Flow

The previous discussions enable the proposal of a design procedure that requires very little iteration and results in a very robust *LCL*-filter. The procedure's steps, illustrated in 6, are as follows:

1) Start with power converter parameters: the rated power S_n, rated ac voltage V_n, rated grid frequency f_n Hz, dc link voltage v_{DC} and switching frequency f_{sw}.
2) Select the active damping procedure: determine the ratio between switching and resonance frequency r_f as discussed in Section III. For the lead-lag network method, r_f should be around 3.3; for the capacitor current feedback method it should be around 3.1, as was shown previously. Higher ratios should be used if passive damping is chosen, as was shown in (29).
3) Select the ratio between grid and converter inductance values r_l, as discussed in Section III.B. Selecting $r_l = 1$ results in the minimum voltage drop and is economically advantageous ($L = L_g$); higher ratios result in increased robustness in response to grid inductance variations, as shown in (16a).
4) For the different values of r_q, plot the total inductance L_T with the help of (23), taking into account that $L_T =$

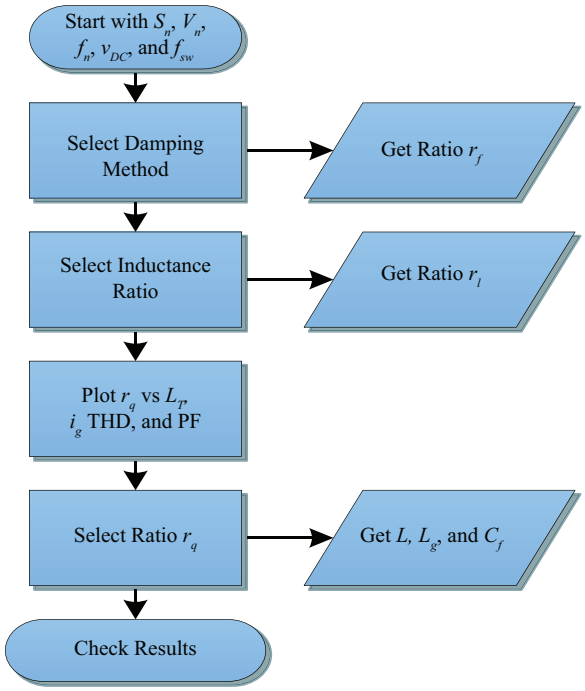

Fig. 6. Design flow for the *LCL*-filter.

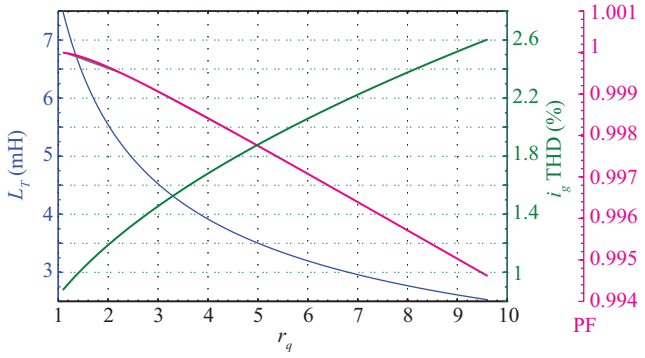

Fig. 7. Total inductance L_T, power factor PF and grid current THD for the different values of r_q when using capacitor current feedback.

$l_T L_b$, the grid current THD using (28), and the power factor using (19) and (20).

5) The minimum $r_q = 1$, with no reactive power consumption, as discussed in Section III.C, and results in overly elevated L_T when compared to the case of the single *L*-filter. In order to select the proper r_q, the power factor should be less than 0.995 and the grid current THD should be below limit 5% and have sufficient margin to account for the non-modeled elements. With all the ratios selected (r_f, r_l, and r_q), the values for L, L_g and C_f can be obtained.
6) Check the results considering non-ideal power devices, passive elements, dc link voltage and grid voltage.

B. Example

Step 1: The grid converter has rated $S_n = 2.2$ kW, $V_n = 380$ V, $f_n = 50$ Hz and $f_{sw} = 8$ kHz. The dc link voltage is usually selected as a 15% over the diode bridge voltage so $v_{DC} = 650$ V.

Step 2: The example will be for both active damping methods the capacitor current feedback, $r_f = 3.12$, and the lead-lag network, $r_f \approx 3.2$–3.4.

Step 3: To attain minimal voltage drop and only one inductor model, the inductance ratio $r_l = 1$ ($L = L_g$) is selected.

Steps 4-5: For the case of the capacitor current feedback, Fig. 7 shows the total inductance L_T, the grid current THD, and the power factor when varying r_q. Selecting $r_q = 1$ results in $C_f = 1.9\,\mu$F and $L = L_g = 4.1$ mH. This would result in no reactive power and no over-rate, but the inductors are excessively large. The total inductance ($L_T = L + L_g$) is almost that required for the converter when using a simple *L*-filter. To calculate the required inductor for the case of the simple *L*-filter, the same formula as in (25a) can be used, after replacing $\tilde{i}_c^{low}$ with the $\tilde{i}_g$. When $r_q = 6.1$ is selected, the resulting $C_f = 4.7\,\mu$F does not produce very much reactive power, with PF = 0.9967, and the resulting inductance values are moderate: $L = L_g = 1.6$ mH, with THD equal to 2%. In the case of the lead-lag network with $r_f = 3.3$, selecting $r_q = 1$ results in $C_f = 2\,\mu$F and again in excessively large inductors: $L = L_g = 4.3$ mH. When selecting $r_q = 5.5$, the resulting $C_f = 4.7\,\mu$F does not produce very much reactive power, with PF = 0.9968, and the resulting inductance values are also moderate: $L = L_g = 1.8$ mH, with THD well bellow 5%.

V. Simulation Results

Fig. 8a shows the root locus in the *z*-plane for the closed loop poles of the current control by varying k_d in the case of the capacitor current feedback. The current control comprises the PI controller and the active damping mechanism; details on the discretization can be found in [6]. The plant includes the inductor resistances, and the PI controllers are tuned according to (1)-(2). It can be seen that the damping for the resonance poles can be selected at will by increasing the gain k_d. Damping the resonance poles too much would not be appropriate, as it would result in excessive control effort; a damping factor equal to $\zeta = 0.1$ is adequate [6]. The simulations consider ideal power devices and passive elements with rated parameters. The grid current THD is equal to 1.8% according to simulations, consistent with the upper bound for the grid current THD, which is 2.17% according to (26). Fig. 9a shows the root locus in the *z*-plane for varying L_g from 40% to 1000%. The minimum value of 40% for L_g was selected considering inaccuracies in the measurements, temperature variations and aging effects. The maximum value of 1000 for L_g was selected considering the line impedance in a weak grid and the presence of many parallel converters. The system remains stable for the full variation range. Hence, the proposed procedure for the capacitor current feedback is very robust when faced with grid inductance variations. Simulation waveforms for the grid current and capacitor voltage are shown in Fig. 10. Some resistance was added to the grid inductor to emulate the behavior of the resistive grid. This provides some damping but there is still resonant oscillation in the

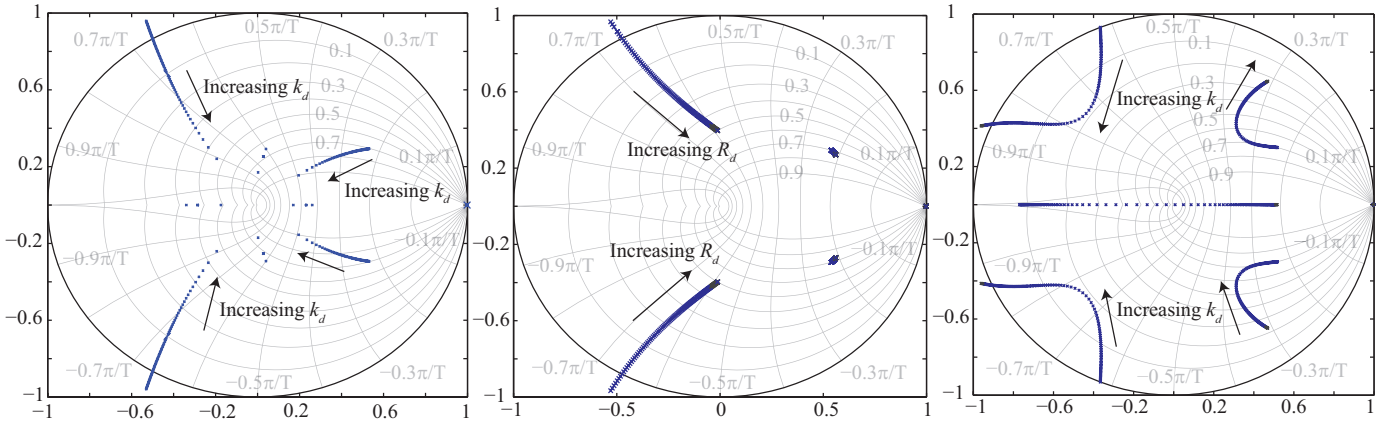

Fig. 8. Root locus in the z-plane by varying a) k_d for active damping with capacitor current feedback, b) R_d for passive damping and c) k_d for active damping with the lead-lag network.

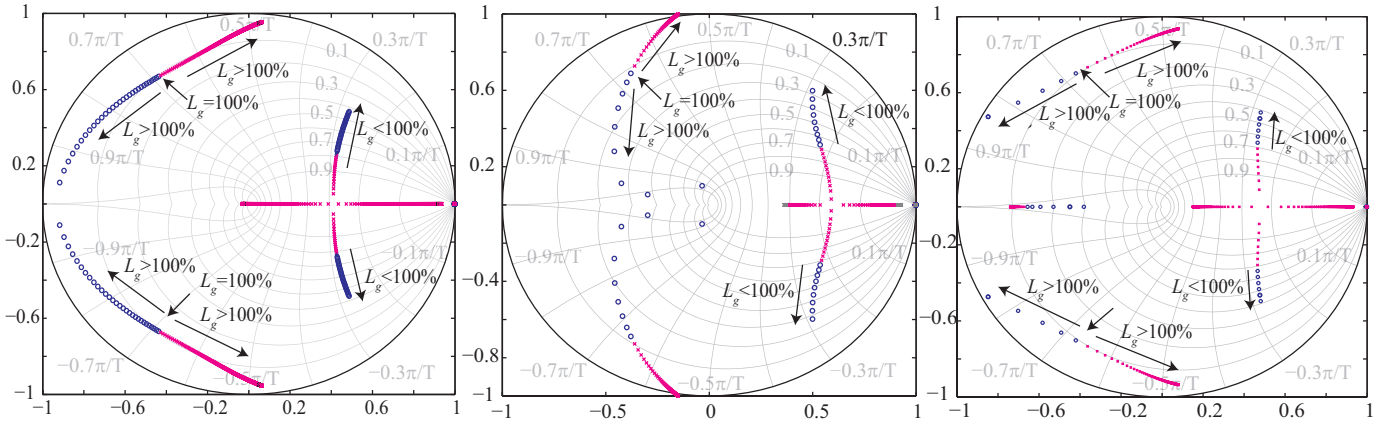

Fig. 9. Root locus in the z-plane by varying L_g from 40% to 1000% for a) active damping with capacitor current feedback b) passive damping and c) active damping with the lead-lag network.

grid current and voltage capacitor that disappears upon the connection of the active damping mechanism. At $t = 0.1$ s, an additional grid inductor of 1.5 mH is added; this small increment in the grid inductance is only slightly noticeable. At $t = 0.15$ s, an additional grid inductor of 6.9 mH is added; the simulation shows that the system is still stable.

Fig. 8b shows the root locus in the z-plane for the closed loop system by varying R_d when using passive damping. It can be seen that, as expected, the behavior is very similar to that of the capacitor current feedback. To get the same previous damping factor $\zeta = 0.1$, the damping resistor should be equal to $R_d = 4.7\ \Omega$. Apart from additional losses and encumbrances, the grid current THD is increased up to 4% according to simulations. This is because zero at $z = 1/R_dC_f$ in the the transfer function between the grid current and converter voltage, which decreases the attenuation. Fig. 9b shows the root locus in the z-plane for varying L_g from 40% to 1000%. It can be seen that the equivalent passive system is less robust against the grid inductance variations, as it results in instability for L_g that is over 4.5 times greater than the rated grid inductance.

Fig. 8c shows the root locus in the z-plane for the closed loop system in the case of the lead-lag network. This procedure (see [19] for details) approximates the derivative of the capacitor voltage (i.e. the capacitor current) by means of a lead-lag network. Hence, increasing k_d allows the pole damping to be increased, but only to a certain extent. Simulations for rated parameters result in a grid current THD equal to 2%. As explained previously, (26) is not so accurate for the case of the lead-lag network and results in a grid current THD of 1.5%; however, it is sufficient for a first approximation. Fig. 9c shows the root locus in the z-plane for varying L_g from 40% to 1000% (ten times), with the system also remaining stable for the full range. Simulations for the grid current and the capacitor voltage are shown in Fig. 11 upon the connection of the active damping mechanism for the rated parameters. Again, at $t = 0.1$ s, an additional grid inductor of 1.2 mH is added without noticeable effect and finally, at $t = 0.15$ s, an additional grid inductor of 6.9 mH is added with the system remaining stable.

It can be seen in Fig. 8a and Fig. 8b, that the active damping affects the low frequency poles while the passive damping, Fig. 8b, does not. For the case of the capacitor current feedback, Fig. 8a, the low frequency poles result in greater damping. For the case of the lead-lag network, elevated values of k_d can cause the low frequency poles to have little damping with

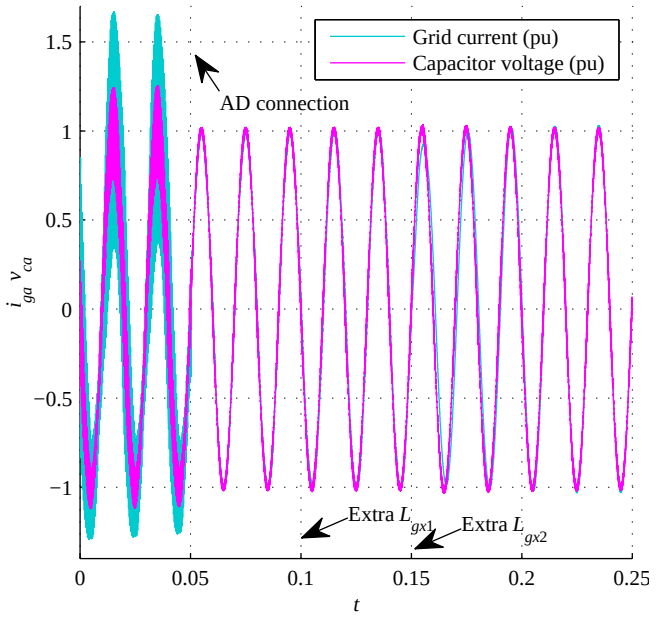

Fig. 10. Grid and converter currents for active damping with capacitor current feedback (simulation results).

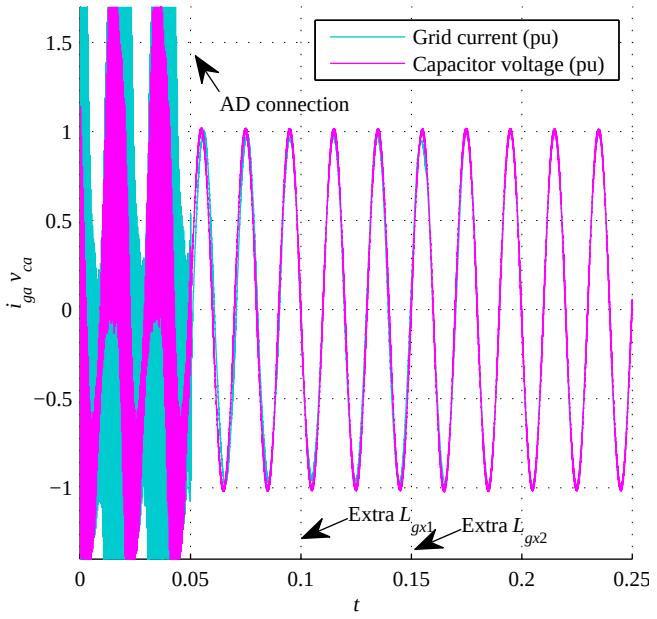

Fig. 11. Grid and converter currents for active damping with the lead-lag network (simulation results).

large overshoot. In such cases, it may be necessary to reduce the proportional gain at the expense of reducing the bandwidth [19]. However, by limiting the damping of the resonance poles to $\zeta = 0.1$, as explained previously, the variations in the location of the low frequency poles are very small and the proportional gain reductions, if needed, are also very small.

VI. Experimental Results

Table I shows the parameters employed in the experimental setup, which is depicted in Fig. 12. The dc link is supplied

TABLE I
Parameters of the Experimental Set-up

Parameter	Symbol	Value
Rated power	S_n	2.2 kVA
Rated ac voltage	V_n	380 V
Rated frequency	f_n	50 Hz
dc link voltage	v_{DC}	650 V
Sampling frequency	f_s	8 kHz
PWM frequency	f_{sw}	8 kHz
Converter inductor	L	1.8 mH
Filter capacitor	C_f	4.7 µF
Grid inductor	L_g	1.8 mH
Resonance frequency	f_{res}	2.447 kHz
Extra Grid inductance 1	L_{gx1}	1.2 mH
Extra Grid inductance 2	L_{gx2}	6.9 mH

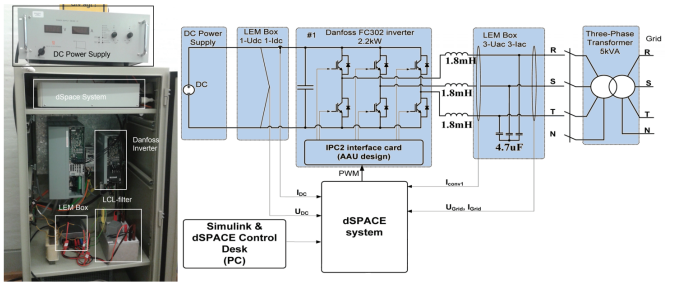

Fig. 12. Set-up used for the experiments.

by a programmable power source. The dc source by Delta Elektronika is unidirectional, so the power flows from the dc link to the grid. The Danfoss FC302 converter is directly connected to the grid through an isolating transformer, the leakage inductance of which corresponds to L_g. The overall system is controlled by means of a dSpace DS1103 controller board. The sign convention for the experiments is the same as in Fig. 2, with positive grid current toward the grid. Only this set-up will be used and the discrepancies with the rated parameters are considered inaccuracies. This approach allows the robustness of the *LCL*-filter design to be assessed.

For the case of the capacitor current feedback, the converter inductance is a little larger than the design value and the real grid inductance is almost double the design value. The resistive distribution grid provides damping and initially, even though the current resonates, the closed loop control is stable. However, the component at the resonance frequency is prominent, which indicates that there is not sufficient damping. Upon the connection of the capacitor current feedback, the oscillation is canceled due to the active damping, and regardless of the parameter inaccuracies, see Fig. 13, proving the correctness of the proposed design formulas.

To further test the robustness of the proposed procedure, additional inductors of 6.9 mH are inserted between the converter and the isolated transformer. In this condition and without the capacitor current feedback, the damping provided by the resistive distribution grid is unable to stabilize the current control and the system trips. Therefore, the overall system must be started with the active damping connected. The experiment shown in Fig. 14 goes from inactive gate drivers to full rated generation. Initially, the grid current corresponds to

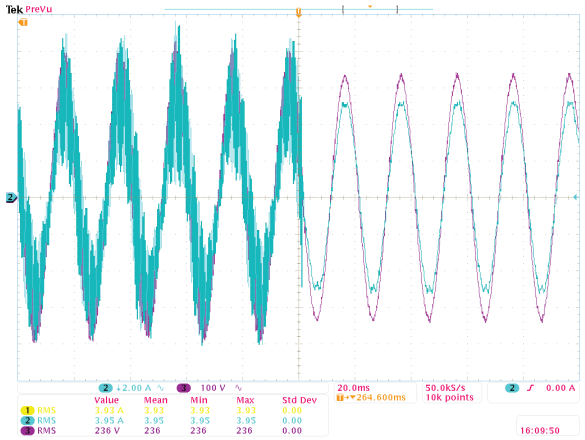

Fig. 13. Capacitor voltage and grid current upon the connection of the capacitor current feedback.

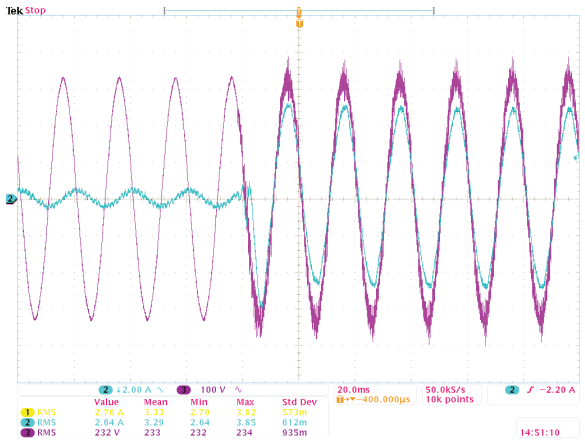

Fig. 14. Capacitor voltage and grid current from disconnection to connection of the *LCL*-filter based converter for active damping with capacitor current feedback.

the current absorbed by the filter capacitor. The system results in stable operation upon the activation of the gate driver. This demonstrates the effectiveness of the proposed procedure and its robust operation even under extreme operating conditions.

For the case of the lead-lag network, the experiment with an additional 6.9 mH inductors is presented in Fig. 15. Again, without the lead-lag network, the damping provided by the resistive distribution grid is unable to stabilize the current control and the system trips. When starting the experiment with the active damping connected, it can be seen that the grid current displays considerable oscillation at the resonance frequency. However, the current control remains stable and the system does not trip. The reason for this is that even though the systems is stable, the damping is very small. Hence, the system is not able to damp the oscillations triggered by the non-linear effects, such as the inductor saturation, which were not modeled in the simulations. This effect is more pronounced in the case of the lead-lag network because it is a less robust method than is the capacitor current feedback and because of the lower accuracy and bandwidth of the voltage sensors, which were designed mainly for grid synchronization.

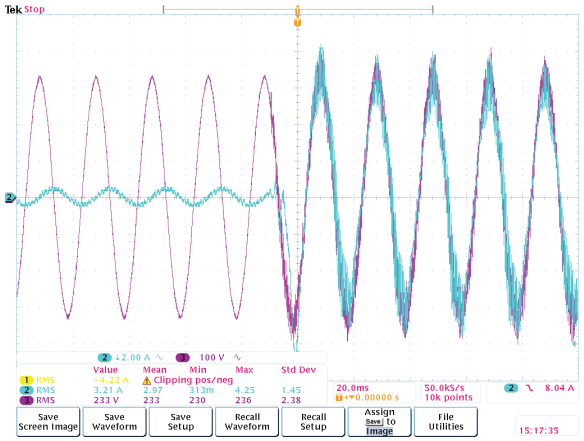

Fig. 15. Capacitor voltage and grid current from disconnection to connection of the *LCL*-filter based converter for active damping with the lead-lag network.

VII. Conclusion

This paper proposes a design flow for *LCL*-filters with robust active damping that requires little iteration and no complex algorithm. The design formulas provide insight and ease the design trade-offs. The ratio between the frequency and resonance frequency depends on the damping procedure. The ratio between the grid and converter inductance affects the filter voltage drop and the resonance frequency variation. The filter capacitor should not produce excessive reactive power to prevent over-rating the converter. The designs parameters obtained resulted in very robust operation with the system remaining stable even for a grid inductance five times the rated value. This makes the proposed procedures adequate for wind parks and solar farms located in remote rural areas that have weak grids and numerous converters in parallel, and that are therefore subject to large grid inductance variations.

References

[1] A. Zobaa and S. Abdel Aleem, "A new approach for harmonic distortion minimization in power systems supplying nonlinear loads," *IEEE Trans. Ind. Informatics*, vol. PP, no. 99, pp. 1–1, 2014.

[2] J. Guerrero, F. Blaabjerg, T. Zhelev, K. Hemmes, E. Monmasson, S. Jemei, M. Comech, R. Granadino, and J. Frau, "Distributed generation: Toward a new energy paradigm," *IEEE Ind. Electron. Mag.*, vol. 4, no. 1, pp. 52 –64, march 2010.

[3] J. He and Y. W. Li, "Hybrid voltage and current control approach for dg-grid interfacing converters with lcl filters," *IEEE Trans. Ind. Electron.*, vol. 60, no. 5, pp. 1797–1809, 2013.

[4] Y. Tang, P. C. Loh, P. Wang, F. H. Choo, F. Gao, and F. Blaabjerg, "Generalized design of high performance shunt active power filter with output lcl filter," *IEEE Trans. Ind. Electron.*, vol. 59, no. 3, pp. 1443–1452, 2012.

[5] J. Yin, S. Duan, and B. Liu, "Stability analysis of grid-connected inverter with lcl filter adopting a digital single-loop controller with inherent damping characteristic," *IEEE Trans. Ind. Informatics*, vol. 9, no. 2, pp. 1104–1112, May 2013.

[6] M. Liserre, A. Dell'Aquila, and F. Blaabjerg, "Stability improvements of an lcl-filter based three-phase active rectifier," in *2002 IEEE 33rd Annu. Power Electron. Specialists Conf., 2002. pesc 02.*, vol. 3, 2002, pp. 1195 – 1201 vol.3.

[7] W. Wu, Y. He, T. Tang, and F. Blaabjerg, "A new design method for the passive damped lcl and llcl filter-based single-phase grid-tied inverter," *IEEE Trans. Ind. Electron.*, vol. 60, no. 10, pp. 4339–4350, 2013.

[8] R. Teodorescu, M. Liserre, and P. Rodriguez, *Grid Converters for Photovoltaic and Wind Power Systems*. Wiley-IEEE press, 2011.

[9] M. Liserre, F. Blaabjerg, and S. Hansen, "Design and control of an lcl-filter-based three-phase active rectifier," *IEEE Trans. Ind. Applicat.*, vol. 41, no. 5, pp. 1281 – 1291, sept.-oct. 2005.
[10] M. Liserre, F. Blaabjerg, and A. DellAquila, "Step-by-step design procedure for a grid-connected three-phase pwm voltage source converter," *International Journal of Electronics*, vol. 91, no. 8, pp. 445–460, 2004.
[11] A. Reznik, M. Simoes, A. Al-Durra, and S. Muyeen, "Lcl filter design and performance analysis for grid-interconnected systems," *IEEE Trans. Ind. Applicat.*, vol. 50, no. 2, pp. 1225–1232, March 2014.
[12] K. Jalili and S. Bernet, "Design of lcl filters of active-front-end two-level voltage-source converters," *IEEE Trans. Ind. Electron.*, vol. 56, no. 5, pp. 1674–1689, 2009.
[13] P. Channegowda and V. John, "Filter optimization for grid interactive voltage source inverters," *IEEE Trans. Ind. Electron.*, vol. 57, no. 12, pp. 4106 –4114, dec. 2010.
[14] J. Muhlethaler, M. Schweizer, R. Blattmann, J. Kolar, and A. Ecklebe, "Optimal design of lcl harmonic filters for three-phase pfc rectifiers," *IEEE Trans. Power Electron.*, vol. 28, no. 7, pp. 3114–3125, 2013.
[15] D. Pan, X. Ruan, C. Bao, W. Li, and X. Wang, "Magnetic integration of the lcl filter in grid-connected inverters," *IEEE Trans. Power Electron.*, vol. 29, no. 4, pp. 1573–1578, April 2014.
[16] Q. Liu, L. Peng, Y. Kang, S. Tang, D. Wu, and Y. Qi, "A novel design and optimization method of an lcl filter for a shunt active power filter," *IEEE Trans. Ind. Electron.*, vol. 61, no. 8, pp. 4000–4010, Aug 2014.
[17] M. Hanif, V. Khadkikar, W. Xiao, and J. Kirtley, "Two degrees of freedom active damping technique for an lcl filter based grid connected pv systems," *IEEE Trans. Ind. Electron.*, vol. PP, no. 99, pp. 1–1, 2013.
[18] M. Orellana and R. Grino, "On the stability of discrete-time active damping methods for vsi converters with a lcl input filter," in *IECON 2012 - 38th Annu. Conf. IEEE Ind. Electron. Soc.*, oct. 2012, pp. 2378 –2383.
[19] R. Peña Alzola, M. Liserre, F. Blaabjerg, R. Sebastian, J. Dannehl, and F. Fuchs, "Systematic design of the lead-lag network method for active damping in lcl-filter based three phase converters," *IEEE Trans. Ind. Informat.*, vol. 10, no. 1, pp. 43–52, Feb 2014.
[20] M. Liserre, A. Dell'Aquila, and F. Blaabjerg, "Genetic algorithm-based design of the active damping for an lcl-filter three-phase active rectifier," *IEEE Trans. Power Electron.*, vol. 19, no. 1, pp. 76 – 86, jan. 2004.
[21] J. Dannehl, M. Liserre, and F. Fuchs, "Filter-based active damping of voltage source converters with lcl filter," *IEEE Trans. Ind. Electron.*, vol. 58, no. 8, pp. 3623 –3633, aug. 2011.
[22] V. Blasko and V. Kaura, "A novel control to actively damp resonance in input lc filter of a three-phase voltage source converter," *IEEE Trans. Ind. Applicat.*, vol. 33, no. 2, pp. 542 –550, mar/apr 1997.
[23] J. Dannehl, F. Fuchs, S. Hansen, and P. Thgersen, "Investigation of active damping approaches for pi-based current control of grid-connected pulse width modulation converters with lcl filters," *IEEE Tran. Ind. Applicat.*, vol. 46, no. 4, pp. 1509 –1517, july-aug. 2010.
[24] A. Hava, T. Lipo, and W. Erdman, "Utility interface issues for line connected pwm voltage source converters: a comparative study," in *Conf. Proc. Tenth Annu. Applied Power Electron. Conf. and Expo., 1995. APEC '95.*, no. 0, mar 1995, pp. 125 –132 vol.1.
[25] M. Liserre, R. Teodorescu, and F. Blaabjerg, "Stability of photovoltaic and wind turbine grid-connected inverters for a large set of grid impedance values," *IEEE Trans. Power Electron.*, vol. 21, no. 1, pp. 263–272, Jan 2006.
[26] S. Parker, B. McGrath, and D. Holmes, "Regions of active damping control for lcl filters," in *2012 IEEE Energy Conversion Congr. and Expo. (ECCE)*, sept. 2012, pp. 53 –60.
[27] B. Bahrani, M. Vasiladiotis, and A. Rufer, "High-order vector control of grid-connected voltage source converters with lcl-filters," *IEEE Trans. Ind. Electron.*, vol. PP, no. 99, pp. 1–1, 2013.
[28] F. Huerta, D. Pizarro, S. Cobreces, F. Rodriguez, C. Giron, and A. Rodriguez, "Lqg servo controller for the current control of lcl grid-connected voltage-source converters," *IEEE Trans. Ind. Electron.*, vol. 59, no. 11, pp. 4272–4284, 2012.
[29] S. Eren, M. Pahlevaninezhad, A. Bakhshai, and P. Jain, "Composite nonlinear feedback control and stability analysis of a grid-connected voltage source inverter with lcl filter," *IEEE Trans. Ind. Electron.*, vol. 60, no. 11, pp. 5059–5074, 2013.
[30] J. Massing, M. Stefanello, H. Grundling, and H. Pinheiro, "Adaptive current control for grid-connected converters with lcl filter," *IEEE Trans. Ind. Electron.*, vol. 59, no. 12, pp. 4681–4693, 2012.
[31] P. Dahono, "A method to damp oscillations on the input lc filter of current-type ac-dc pwm converters by using a virtual resistor," in *The 25th Int. Telecommun. Energy Conf., 2003. INTELEC '03.*, oct. 2003, pp. 757 –761.
[32] hidden names, "Robust design of lcl-filters for active damping in grid converters," in *Industrial Electronics Society, IECON 2013 - 39th Annual Conference of the IEEE*, Nov 2013, pp. 1248–1253.
[33] C. Bao, X. Ruan, X. Wang, W. Li, D. Pan, and K. Weng, "Step-by-step controller design for lcl-type grid-connected inverter with capacitor current-feedback active-damping," *IEEE Trans. Power Electron.*, vol. 29, no. 3, pp. 1239–1253, March 2014.
[34] R. Peña Alzola, M. Liserre, F. Blaabjerg, M. Ordonez, and T. Kerekes, "A self-commissioning notch filter for active damping in a three-phase lcl -filter-based grid-tie converter," *IEEE Trans. Power Electron.*, vol. 29, no. 12, pp. 6754–6761, Dec 2014.
[35] M. Kabir, Y. Mishra, G. Ledwich, Z. Dong, and K. Wong, "Coordinated control of grid connected photo voltaic reactive power and battery energy storage systems to improve the voltage profile of a residential distribution feeder," *IEEE Trans. Ind. Informatics*, vol. PP, no. 99, pp. 1–1, 2014.
[36] F. Jurado, C. Garcia, L. Fernandez, F. Llorens, and F. Jurado, "Anfis-based control of a grid-connected hybrid system integrating renewable energies, hydrogen and batteries," *IEEE Trans. Ind. Informatics*, vol. PP, no. 99, pp. 1–1, 2013.
[37] J. Agorreta, M. Borrega, J. Lopez, and L. Marroyo, "Modeling and control of n -paralleled grid-connected inverters with lcl filter coupled due to grid impedance in pv plants," *IEEE Trans. Power Electron.*, vol. 26, no. 3, pp. 770 –785, march 2011.
[38] H. Ginn and G. Chen, "Digital control method for grid-connected converters supplied with nonideal voltage," *IEEE Trans. Ind. Informatics*, vol. 10, no. 1, pp. 127–136, Feb 2014.
[39] V. Blasko and V. Kaura, "A new mathematical model and control of a three-phase ac-dc voltage source converter," *IEEE Trans. Power Electron.*, vol. 12, no. 1, pp. 116–123, Jan 1997.
[40] R. Peña Alzola, M. Liserre, F. Blaabjerg, R. Sebastian, J. Dannehl, and F. Fuchs, "Analysis of the passive damping losses in lcl-filter-based grid converters," *IEEE Trans. Power Electron.*, vol. 28, no. 6, pp. 2642 – 2646, june 2013.
[41] W. Yang, W. Cao, T. Chung, and J. Morris, *Applied Numerical Methods Using Matlab*. Wiley-Interscience, 2005.
[42] C. L. Phillips and R. D. Harbor, *Feedback Control Systems*. Prentice Hall, 2000.

Rafael Peña Alzola Rafael Peña-Alzola received the combined licentiate and M.Sc. degree in industrial engineering from the University of the Basque Country, Bilbao, Spain, in 2001, and the Ph.D. degree from the National University for Distance Learning, UNED, Madrid, Spain, in 2011. He has worked as an electrical and control engineer for several companies in Spain. From September 2012 to July 2013, he has been Guest Postdoc in the Department of Energy Technology at Aalborg University, Aalborg, Denmark.

Since August 2013 he is Postdoc Research Fellow at the Department of Electrical and Computer Engineering at The University of British Columbia (UBC) in Vancouver, Canada. His research interests are energy storage, LCL-filters, solid-state transformers and innovative control techniques for power converters.

Marco Liserre Marco Liserre (S'00-M'02-SM'07-F13) received the MSc and PhD degree in Electrical Engineering from the Bari Polytechnic, respectively in 1998 and 2002. He has been Associate Professor at Bari Polytechnic and Professor in reliable power electronics at Aalborg University (Denmark). He is currently Full Professor and he holds the Chair of Power Electronics at Christian-Albrechts-University of Kiel (Germany). He has published 168 technical papers (44 of them in international peer-reviewed journals), 3 chapters of a book and a book (Grid Converters for Photovoltaic and Wind Power Systems, ISBN-10: 0-470-05751-3 IEEE-Wiley, also translated in Chinese). These works have received more than 6000 citations. He has been recently awarded with an ERC Consolidator Grant for an overall budget of 2 MEuro for the project The Highly Efficient And Reliable smart Transformer (HEART), a new Heart for the Electric Distribution System.

He is member of IAS, PELS, PES and IES. He is Associate Editor of the IEEE Transactions on Industrial Electronics, IEEE Industrial Electronics Magazine, IEEE Transactions on Industrial Informatics, where he is currently Co-Eic, IEEE Transactions on power electronics and IEEE Journal of Emerging and Selected Topics in Power Electronics. He has been Founder and Editor-in-Chief of the IEEE Industrial Electronics Magazine, Founder and the Chairman of the Technical Committee on Renewable Energy Systems, Co-Chairman of the International Symposium on Industrial Electronics (ISIE 2010), IES Vice-President responsible of the publications. He has received the IES 2009 Early Career Award, the IES 2011 Anthony J. Hornfeck Service Award, the 2011 Industrial Electronics Magazine best paper award and the Third Prize paper award by the Industrial Power Converter Committee at ECCE 2012, 2012. He is senior member of IES AdCom. In 2013 he has been elevated to the IEEE fellow grade with the following citation for contributions to grid connection of renewable energy systems and industrial drives.

Frede Blaabjerg Frede Blaabjerg (S'86-M'88-SM'97-F'03) was with ABB-Scandia, Randers, Denmark, from 1987 to 1988. From 1988 to 1992, he was a Ph.D. Student with Aalborg University, Aalborg, Denmark. He became an Assistant Professor in 1992, an Associate Professor in 1996, and a Full Professor of power electronics and drives in 1998. His current research interests include power electronics and its applications such as in wind turbines, PV systems, reliability, harmonics and adjustable speed drives.

He has received 15 IEEE Prize Paper Awards, the IEEE PELS Distinguished Service Award in 2009, the EPE-PEMC Council Award in 2010 and the IEEE William E. Newell Power Electronics Award 2014. He was an Editor-in-Chief of the IEEE TRANSACTIONS ON POWER ELECTRONICS from 2006 to 2012. He has been Distinguished Lecturer for the IEEE Power Electronics Society from 2005 to 2007 and for the IEEE Industry Applications Society from 2010 to 2011.

Martin Ordonez Martin Ordonez (S'02 - M'09) was born in Neuquen, Argentina. He received the Ing. degree in electronics engineering from the National Technological University, Argentina, in 2003, and the M.Eng. and Ph.D. degrees from Memorial University of Newfoundland (MUN), Canada, (2006 and 2009).

He is an Assistant Professor and Canada Research Chair at the University of British Columbia (UBC), Vancouver, BC, Canada. He is also an Adjunct Professor with Simon Fraser University and MUN, Canada. His industrial experience includes R&D at Xantrex Technology Inc./Elgar Electronics Corp. (now AMETEK Programmable Power), Deep-Ing Electronica de Potencia and TRV Dispositivos (Argentina).

Dr. Ordonez is an Associate Editor of the IEEE TRANSACTIONS ON POWER ELECTRONICS, serves on several IEEE committees, and reviews widely for IEEE/IET. He was awarded the David Dunsiger Award for Excellence (2009), the Chancellors Graduate Award/Birks Graduate Medal (2006), and became a Fellow of the School of Graduate Studies, MUN.

Yongheng Yang Yongheng Yang (S'12-M'15) received the B.Eng. degree in electrical engineering and automation from Northwestern Polytechnical University, Xi'an, China, in 2009 and the PhD degree in electrical engineering from Aalborg University, Aalborg, Denmark, in 2014. During 2009-2011, he was working towards the master-doctoral degree in the School of Electrical Engineering at Southeast University, Nanjing, China, where he was involved in the modeling and control of single-phase grid-connected photovoltaic (PV) systems. From March to May in 2013, he was a Visiting Scholar in the Department of Electrical and Computer Engineering at Texas A&M University, College Station, TX, USA.

He is currently a Postdoc in the Department of Energy Technology at Aalborg University, Aalborg East, Denmark. His research interests include grid detection, synchronization, control of single-phase photovoltaic systems in different operation modes, reliability for next-generation PV inverters, and harmonics in adjustable speed drives and grid-connected converters.